INTERNATIONAL JOURNAL FOR NUMERICAL METHODS IN FLUIDS
Int. J. Numer. Meth. Fluids 2000; **34**: 685–700

Optimal design of paper machine headboxes

J. Hämäläinen[a,1], R. A. E. Mäkinen[b,2] and P. Tarvainen[c,*,3]

[a] *Valmet Corporation, PO Box 587, FIN-40101 Jyväskylä, Finland*
[b] *Department of Mathematical Information Technology, University of Jyväskylä, PO Box 35, FIN-40351 Jyväskylä, Finland*
[c] *Numerola Oy (Limited), Väinönkatu 11A, FIN-40100 Jyväskylä, Finland*

SUMMARY

A shape optimization problem for incompressible flows within a stabilized finite element framework is studied. The goal is to develop and test numerical realizations of optimal shape design problems that could be applied to non-trivial industrial problems. The resulting algorithm is applied to the optimization of the geometry of a tapered header in a paper machine headbox. Copyright © 2000 John Wiley & Sons, Ltd.

KEY WORDS: optimal shape design; paper machine headbox; shape optimization

1. INTRODUCTION

The headbox is the first component in the paper making process on a paper machine, located at the wet end (Figure 1). Fluid flow phenomena taking place in the headbox largely determine the quality of paper produced, e.g., the basis weight and the fiber orientation variations. The first flow passage in the headbox is a tapered header (Figure 2). The header is designed to distribute fiber suspension (wood fibers, filler clays and chemicals mixed in water) so that the produced paper will have an optimal basis weight (thickness) and fiber orientation across the width of a paper machine.

Considerable progress has been made in the mathematical modeling and numerical computations related to paper machine technology; see, for instance, References [1–3]. However, until now, very little attention has been given to the question of controlling physical flow situations, for example, shape optimization problems governed by flow equations.

The shape optimization problem considered in this paper is to find optimal tapering of the header such that the outlet flow rate distribution from the headbox will result in optimal paper

* Correspondence to: Numerola Oy (Limited), Väinönkatu 11A, FIN-40100 Jyväskylä, Finland.
[1] E-mail: jari.p.hamalainen@valmet.com
[2] E-mail: rainom@mit.jyu.fi
[3] E-mail: pasi.tarvainen@numerola.fi

Received July 1999
Revised December 1999

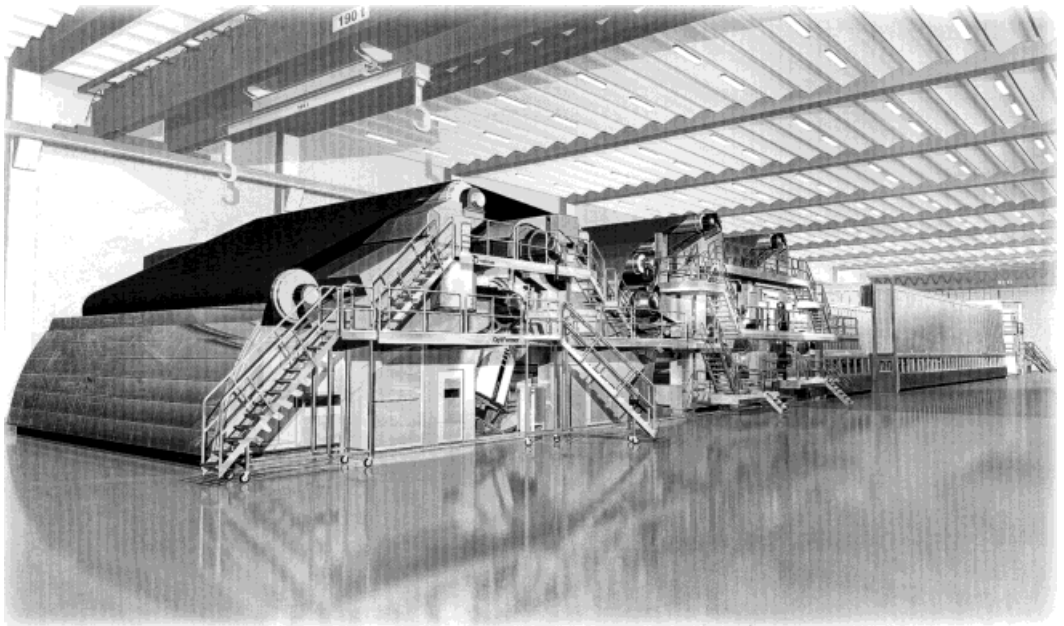

Figure 1. Valmet OptiConcept paper machine.

quality, i.e., the back wall (see Figure 2) of the header is optimally designed in order to obtain a desired velocity on the outflow boundary.

Mathematically, the shape optimization problem is to minimize, through a variation of the domain boundary or a part of it, an objective function subject to constraints imposed by a boundary value problem, as well as other physical and geometrical conditions. Conventional trial-and-error design methods often prove to be time-consuming, expensive and ineffective in addressing such design problems. Over the last 20 years, optimal shape design algorithms have been developed for many structural and mechanical systems from the mathematical and engineering point of view, see, for example, References [4,5], while a few papers have been published about applications in fluid dynamics. However, advances in computational fluid dynamics (CFD), numerical optimization methods and high-performance computers have made it possible to develop computer-based systems that will automate the design of such systems.

Most of the existing literature relevant to shape optimization of fluid flows is in the context of aerodynamics, for example, References [6–10]. Aerospace and aeronautical engineering often deal with high-Reynolds number flows with viscosity being ignored and, thus, the fluid flow is modeled by full potential or Euler equations. However, there are many applications where an inviscid assumption is not valid and the full Navier–Stokes equations should be used. Shape optimization governed by viscous incompressible flows have been studied, e.g., see References [11–14]. Also, it is worth mentioning the papers related to shape optimization and

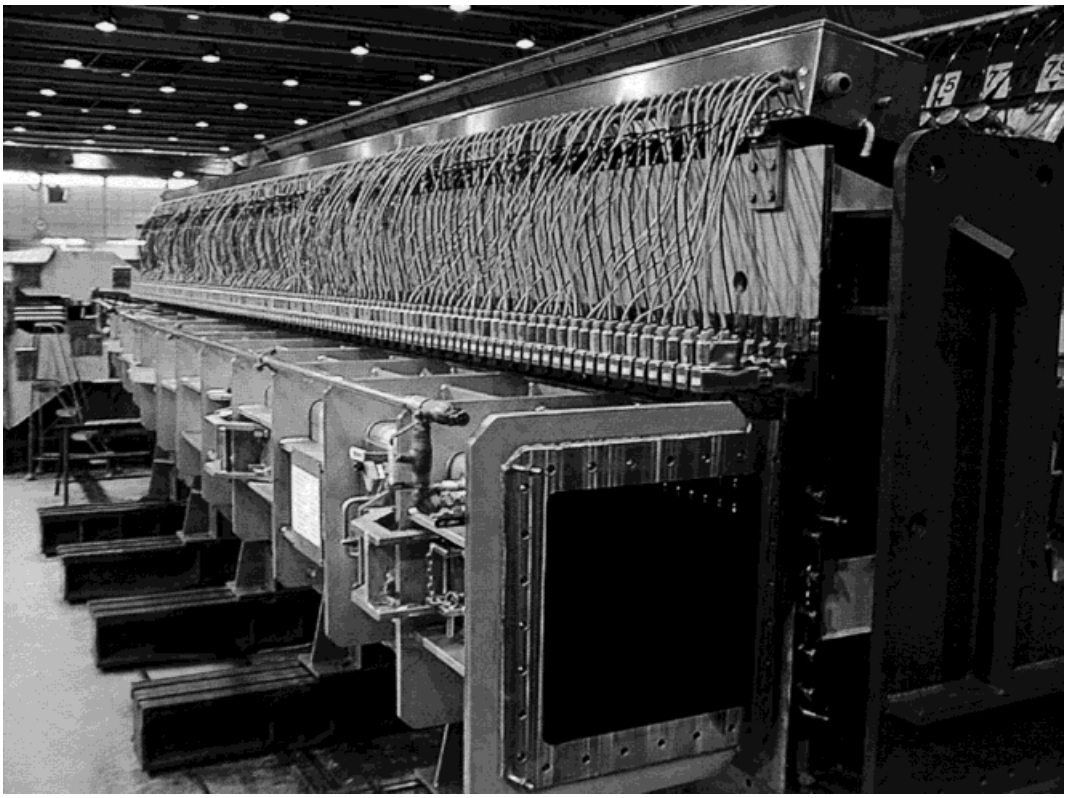

Figure 2. Tapered header.

automatic differentiation in CFD, like in References [15,16]. For further study on numerical methods for shape optimization in fluids, we refer the reader to Reference [5].

In this paper, a shape optimization algorithm for viscous incompressible flows within a *stabilized* finite element framework is presented: The related optimal design problem is formulated as a non-linear optimization problem. The geometric design sensitivity analysis required for the efficient use of non-linear programing methods, like the sequential quadratic programing (SQP)-method, is carried out analytically via the adjoint equation technique. The flow equations are discretized by a stabilized finite element method [17]. The resulting shape optimization algorithm is applied to the geometry design of paper machine headboxes.

The rest of the paper is organized as follows. In Section 2 the flow model as well as the related shape optimization problems are formulated. The discretization procedures used here are described briefly in Section 3. Special attention is given to the sensitivity analysis using the adjoint equation technique in Section 4. In Section 5, various numerical experiments are reported, and concluding remarks are discussed in Section 6.

2. SETTING OF THE PROBLEM

2.1. The flow model

A fluid flowing in a headbox is a mixture of water and wood fibers and, therefore, simulation of separation or mixing of different phases requires a multi-phase model for the water–fibre suspension. For simulation of large-scale phenomena, however, one-phase modeling, where the fluid is pure water, is assumed to be sufficient. A typical Reynolds number is of order 10^6 in the header inlet, requiring turbulence to be taken into account. The header presents some special difficulties in modeling the flow, because the fluid flows from the header to an equalizing chamber through a manifold tube bank consisting of hundreds of small identical tubes. The manifold tube bank must be taken into account in the average. This has been performed by replacing the tube bank by a homogeneous effective medium, which results in a non-linear third type of outflow boundary condition depending on the geometry of the tubes. Detailed descriptions of modeling of the headbox flows and derivation of the homogenized outflow boundary condition is given in References [1–3].

We use a simplified flow model, namely the Reynolds-averaged Navier–Stokes (RANS) equations with a mixing-length turbulence model. The problem is also simplified by modeling only a two-dimensional geometry instead of the real three-dimensional header. More complex models, reported in References [1–3], have been validated for the every-day industrial design applications. However, the simplified model used here represents essentially the same aspects as the real model from the point of view of the optimal design methods.

2.1.1. Basic equations. We consider a two-dimensional fluid flow in a header $\Omega(\alpha)$, as given in Figure 3. The parameters H_1, H_2, L_1, L_2 and L_3 are fixed. Let the back wall of the header $S = S(\alpha) \subset \partial\Omega(\alpha)$ be defined by a smooth function α as

$$S(\alpha) = \{\boldsymbol{x} = (x_1, x_2) \,|\, L_1 \leq x_1 \leq L_1 + L_2,\ x_2 = \alpha(x_1)\}$$

Here, the fluid flow model consists of the time-averaged Reynolds equations

$$\begin{aligned} -\nabla\cdot\boldsymbol{\tau} + \rho\boldsymbol{u}\cdot\nabla\boldsymbol{u} + \nabla p &= 0 \\ \nabla\cdot\boldsymbol{u} &= 0 \end{aligned} \tag{1}$$

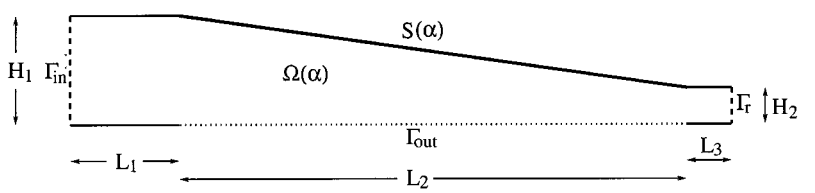

Figure 3. Geometry of a header.

where $\boldsymbol{u} = (u_1, u_2)$ denotes the velocity with u_i being the velocity component in the x_i-direction in a Cartesian co-ordinate system, $i = 1, 2$; and p is the static pressure. The components of the shear stress tensor $\boldsymbol{\tau}$ are

$$\tau_{ij} = \mu\left(\frac{\partial u_i}{\partial x_j} + \frac{\partial u_j}{\partial x_i}\right), \quad i, j = 1, 2 \tag{2}$$

where the viscosity is $\mu = \mu_0 + \mu_T$, i.e., the sum of the dynamic viscosity and the eddy viscosity.

2.1.2. Algebraic turbulence model. In order to solve the Reynolds-averaged equations for turbulent flows, what remains is to select a model for the turbulent viscosity μ_T. Here, we choose a simple algebraic model

$$\mu_T = \rho \ell^2 \left(\frac{1}{2}\varepsilon_{ij}\varepsilon_{ij}\right)^{1/2} \tag{3}$$

with $(\frac{1}{2}\varepsilon_{ij}\varepsilon_{ij})^{1/2}$ being the second invariant of the strain rate tensor

$$\varepsilon_{ij} = \frac{1}{2}\left(\frac{\partial u_i}{\partial x_j} + \frac{\partial u_j}{\partial x_i}\right)$$

and ℓ denotes the mixing length to be determined below.

The mixing length is based on the so-called Nikuradse formula [18,19]

$$\ell_N \equiv \ell(x_1) = \frac{1}{2} H(x_1)\left[0.14 - 0.08\left(1 - \frac{2y(x_1)}{H(x_1)}\right)^2 - 0.06\left(1 - \frac{2y(x_1)}{H(x_1)}\right)^4\right] \tag{4}$$

where $H(x_1)$ and $y(x_1)$ are the separation of walls and the normal distance from the wall at x_1 respectively. Furthermore, to improve the accuracy of the model we introduce the near-wall correction based on the van Driest damping function [19] as follows. Let us determine the value δ_b by

$$\delta_b = d\sqrt{\nu}, \quad \nu = \frac{\mu_0}{\rho} \tag{5}$$

with d being a positive constant to be specified either somehow systemically or experimentally. Now, our algebraic turbulence model is based on the definition of the mixing length as follows:

$$\ell_{\mathrm{VDN}} = \begin{cases} \kappa y\left[1 - \exp\left(-\dfrac{y u_\tau}{A_0^+ \nu}\right)\right], & y \le \delta_b \\ \ell_N, & y > \delta_b \end{cases} \tag{6}$$

where the constant $A_0^+ = 26$ and κ is the von Kármán constant, $\kappa = 0.41$. The friction velocity u_τ is given by $u_\tau = \sqrt{\tau_w/\rho}$, where

$$\tau_w = \mu_0 \left(\frac{\partial u}{\partial y} \right)_w$$

is the wall shear stress.

Remark 1
The value of δ_b denotes an approximation of the boundary layer thickness. The parameter is to be determined according to the flow model.

Remark 2
We made numerical comparisons with the above model and the well-known k–ε model [19] to define the eddy viscosity, i.e.

$$-\nabla \cdot \left[\left(\mu_0 + \frac{\mu_T}{\sigma_k} \right) \nabla k \right] + \rho \boldsymbol{u} \cdot \nabla k = \mu_T \Phi - \rho \varepsilon \tag{7}$$

$$-\nabla \cdot \left[\left(\mu_0 + \frac{\mu_T}{\sigma_\varepsilon} \right) \nabla \varepsilon \right] + \rho \boldsymbol{u} \cdot \nabla \varepsilon = C_1 \frac{\varepsilon}{k} \mu_T \Phi - \rho C_2 \frac{\varepsilon^2}{k} \tag{8}$$

where the eddy viscosity is

$$\mu_T = \rho C_\mu \frac{k^2}{\varepsilon} \tag{9}$$

and

$$\Phi = \sum_{i,j=1}^{2} \left(\frac{\partial u_i}{\partial x_j} + \frac{\partial u_j}{\partial x_i} \right) \frac{\partial u_i}{\partial x_j} \tag{10}$$

According to the numerical experiments reported in Reference [20], the desired properties of actual interest (i.e. the velocity profiles on the outflow boundary, see below) can be almost reached by using the simple zero-equation turbulence model given above. However, from an optimization the point of view, this model is much more favorable than the two-equation model based on the determination of the kinetic energy k and the kinetic energy dissipation ε from Equations (7) and (8).

Remark 3
A simpler turbulence model based on only the use of Nikuradse's formula (4) was used in Reference [21]. According to the numerical comparisons reported in Reference [20], it does not give satisfactory results from the modeling point of view.

2.2. Boundary conditions

For the header flow model, the following boundary conditions are posed, see Figure 3:

$$\boldsymbol{u} = 0, \quad \text{on } \Gamma_0(\alpha) \equiv \partial\Omega(\alpha)\backslash(\Gamma_{\text{in}} \cup \Gamma_{\text{out}} \cup \Gamma_r) \tag{11}$$

$$\boldsymbol{u} = \boldsymbol{u}_{\text{in}}, \quad \text{on } \Gamma_{\text{in}} \tag{12}$$

$$\boldsymbol{u} = \boldsymbol{u}_{\text{r}}, \quad \text{on } \Gamma_{\text{r}} \tag{13}$$

$$p = \Delta p(u_n), \quad \text{on } \Gamma_{\text{out}} \tag{14}$$

where $\Delta p(u_n)$ denotes the pressure losses in the manifold tube bank, typically of the form $\Delta p(u_n) = cu_n^2$, with c being a constant and u_n the normal velocity component. For details, see References [1–3].

2.3. The shape optimization problem

Having the solution $(\boldsymbol{u}, p) = (\boldsymbol{u}(\alpha), p(\alpha))$ on the region $\Omega(\alpha)$, we may set up an optimization problem

$$\min_{\alpha \in U^{\text{ad}}} F(\boldsymbol{u}(\alpha)) \quad \text{subject to Equation (1), (11)} - \text{(14)} \tag{15}$$

where $F(\boldsymbol{u}(\alpha))$ is a cost function measuring the performance of the system and U^{ad} denotes the set of technically admissible functions defining $S(\alpha)$. In our case, the cost function is given by

$$F(\boldsymbol{u}(\alpha)) = \int_{\Gamma_{\text{out}}} (u_2 - \bar{u}_2)^2 \, \mathrm{d}\Gamma \tag{16}$$

where $\boldsymbol{u} = (u_1, u_2)^T$ and $\bar{\boldsymbol{u}} = (\bar{u}_1, \bar{u}_2)^T$ are the simulated and the desired velocities on the outflow boundary Γ_{out} of the header respectively. The cost function is minimized by varying the shape of the back wall $S(\alpha)$.

3. DISCRETIZATION

3.1. The discrete state problem

The state problem (1) is discretized by a stabilized finite element method by using three-noded triangular elements and piecewise linear finite element test functions. Following Reference [17] and having the linearly interpolated velocity approximation, the stabilized finite element method for the flow problem (1) can be written in the form: find $(\boldsymbol{u}_h, p_h)$ such that

$$B(\boldsymbol{u}_h, p_h;\ \boldsymbol{v}, q) = F(\boldsymbol{v}, q) \tag{17}$$

for all test functions $(\boldsymbol{v}, q)$. Here,

$$B(\boldsymbol{u}, p; \boldsymbol{v}, q) = (2\mu\varepsilon(\boldsymbol{u}), \varepsilon(\boldsymbol{v})) + (\rho\boldsymbol{u}\cdot\nabla\boldsymbol{u}, \boldsymbol{v}) - (p, \nabla\cdot\boldsymbol{v}) - (\rho\nabla\cdot\boldsymbol{u}, q) + (\nabla\cdot\boldsymbol{u}, \rho\delta(\boldsymbol{u})\nabla\cdot\boldsymbol{v}) + \sum_e (\rho\boldsymbol{u}\cdot\nabla\boldsymbol{u} + \nabla p, \tau(\boldsymbol{u})(\boldsymbol{u}\cdot\nabla\boldsymbol{v} - \nabla q))$$

and

$$F(\boldsymbol{v}, q) = (\rho\boldsymbol{f}, \boldsymbol{v}) + \sum_e (\rho\boldsymbol{f}, \tau(\boldsymbol{u})(\boldsymbol{u}\cdot\nabla\boldsymbol{v} - \nabla q)) \tag{18}$$

Thus, stabilization of the finite element method consists of adding mesh-dependent terms to the standard Galerkin method, which are residuals of the original equations evaluated elementwise. The stabilization parameters are defined as follows [17]:

$$\delta(\boldsymbol{u}) = \lambda|\boldsymbol{u}|h_K\xi(Re_x), \qquad \tau(\boldsymbol{u}) = \frac{h_K}{2|\boldsymbol{u}|}\,\xi(Re_x)$$

where

$$\xi(Re_x) = \min(Re_x, 1), \qquad Re_x = \frac{\rho m_k|\boldsymbol{u}|h_K}{4\mu}$$

with h_K being the diameter of an element. λ and m_k are positive parameters, here $\lambda = 1$ and $m_k = 1/3$ [17]. Equation (17) is then converted into the system of non-linear algebraic equations

$$\boldsymbol{r}(\boldsymbol{q}) \equiv \boldsymbol{C}(\boldsymbol{q})\boldsymbol{q} - \boldsymbol{b} = \boldsymbol{0} \tag{19}$$

where the vector $\boldsymbol{q}$ contains the nodal values of the velocity and pressure.

System (19) is then solved numerically by using the Newton–Raphson method

$$\boldsymbol{H}(\boldsymbol{q}^k)(\boldsymbol{q}^{k+1} - \boldsymbol{q}^k) = -\boldsymbol{r}(\boldsymbol{q}^k) \tag{20}$$

where

$$\boldsymbol{H}(\boldsymbol{q}) = \frac{\partial\boldsymbol{r}(\boldsymbol{a};\ \boldsymbol{q})}{\partial\boldsymbol{q}}$$

is the Jacobian of $\boldsymbol{r}(\boldsymbol{q})$ with respect to $\boldsymbol{q}$.

3.2. The discrete optimization problem

We use the Bézier curve representation for the back wall $S(\alpha)$ of the header. Using this approach, the boundary is always smooth and the number of the design variables may be kept

moderate. For more details, see Reference [22]. The curve is defined by the control points $z^{(0)}, \ldots, z^{(N+1)}$. The curve interpolates the first and last control points that have fixed values $z^{(0)} = (L_1, H_1)$, $z^{(N+1)} = (L_1 + L_2, H_2)$. The rest of the control points are allowed to move in the x_2-direction within 'moving limits' in the following way:

$$z^{(i)} = \left(L_1 + i\frac{L_2}{N+1},\ (1-a_i)H_2 + a_i H_1 \right), \quad i = 1, \ldots, N$$

Thus, $0 \le a_i \le 1$, $i = 1, \ldots, N$, are the optimization parameters.

After discretization, we have the non-linear optimization problem

$$\min_{\boldsymbol{b}_l \le \boldsymbol{a} \le \boldsymbol{b}_u} F(\boldsymbol{q}(\boldsymbol{a})) = \sum_{i \in I_0} \omega_i (q_i - \bar{q}_i)^2 \quad \text{subject to Equation (19)} \tag{21}$$

with box constraints corresponding to the condition $\alpha \in U^{\mathrm{ad}}$. Here, I_0 is the set of indices corresponding to the mesh nodes x_i on the outflow boundary Γ_{out}, $\bar{q}_i = u_2(x_i)$ and ω_i, $i \in I_0$, are the weights.

Problem (21) can be solved numerically by using any non-linear optimization algorithm. However, the cost function is an implicit function of the design parameters and, therefore, its evaluation requires the solution of the state problem (19). Sequential linear programing, SQP and convex linearization methods have been successfully used to solve shape optimization problems in structural mechanics, for example, see Reference [23]. In general, the mapping $\boldsymbol{a} \mapsto F(\boldsymbol{q}(\boldsymbol{a}))$ is non-convex, and hence only a local minimum of F can be found.

4. SENSITIVITY ANALYSIS

4.1. Adjoint equation technique

We describe the adjoint equation technique by means of the Lagrangian functional formulation [5]. The Lagrangian for problem (21) is defined as follows:

$$\mathscr{L}(\boldsymbol{a}, \boldsymbol{q}, \boldsymbol{p}, \boldsymbol{\eta}, \boldsymbol{\lambda}) \equiv F(\boldsymbol{q}) - \boldsymbol{p}^T \boldsymbol{r}(\boldsymbol{a};\ \boldsymbol{q}) - \boldsymbol{\eta}^T(\boldsymbol{b}_l - \boldsymbol{a}) - \boldsymbol{\lambda}(\boldsymbol{a} - \boldsymbol{b}_u) \tag{22}$$

Then, the optimality conditions for problem (21) read

$$\frac{\partial \mathscr{L}}{\partial a_k} = -\boldsymbol{p}^T \frac{\partial \boldsymbol{r}(\boldsymbol{a};\ \boldsymbol{q})}{\partial a_k} + \eta_k - \lambda_k = 0, \quad k = 1, \ldots, N \tag{23}$$

$$\nabla_{\boldsymbol{q}} \mathscr{L} = \nabla_{\boldsymbol{q}} F(\boldsymbol{q}) - \boldsymbol{H}(\boldsymbol{a};\ \boldsymbol{q})^T \boldsymbol{p} = 0 \tag{24}$$

$$\boldsymbol{\eta}^T(\boldsymbol{b}_l - \boldsymbol{a}) = 0, \quad \boldsymbol{\eta} \ge 0 \tag{25}$$

$$\boldsymbol{\lambda}^T(\boldsymbol{a} - \boldsymbol{b}_u) = 0, \quad \boldsymbol{\lambda} \ge 0 \tag{26}$$

Equations (23) and (24) imply that the partial derivatives of the cost function $F(\boldsymbol{q}(\boldsymbol{a}))$ with respect to design variables can be calculated as

$$\frac{\partial F(\boldsymbol{q}(\boldsymbol{a}))}{\partial a_k} = -\boldsymbol{p}^T \frac{\partial \boldsymbol{r}(\boldsymbol{a};\ \boldsymbol{q})}{\partial a_k}, \quad k = 1, \ldots, N$$

where $\boldsymbol{p}$ is the solution of the (linear) adjoint equation

$$\boldsymbol{H}(\boldsymbol{a};\ \boldsymbol{q})^T \boldsymbol{p} = \nabla_{\boldsymbol{q}} F(\boldsymbol{q}) \tag{27}$$

If the state problem is solved using the Newton–Raphson method (20), the matrix $\boldsymbol{H}(\boldsymbol{a};\ \boldsymbol{q})$ is readily available. Furthermore, the calculation of the gradient requires only one solution of the non-linear flow problem, together with the solution of the linear adjoint equation (27).

4.2. Sensitivity of the residual vector with respect to design

Derivatives of the residual vector $\boldsymbol{r}(\boldsymbol{a}, \boldsymbol{q})$ with respect to geometric design variables can be calculated in a straightforward way using the results presented in References [24,25].

The residual can be computed element by element using the normal assembling procedure

$$\boldsymbol{r} = \sum_e \boldsymbol{P}^e \boldsymbol{r}^e \tag{28}$$

where $\boldsymbol{P}^e$ are the elementwise boolean mapping matrices. Let $\boldsymbol{p}^e = (\boldsymbol{P}^e)^T \boldsymbol{p}$ be the vector containing adjoint degrees of freedom associated with an element Ω_e. Then, we have

$$\frac{\partial F}{\partial a_k} = -\boldsymbol{p}^T \frac{\partial \boldsymbol{r}}{\partial a_k} = -\boldsymbol{p}^T \sum_e \frac{\partial (\boldsymbol{P}^e \boldsymbol{r}^e)}{\partial a_k} = -\sum_e \boldsymbol{p}^T \boldsymbol{P}^e \frac{\partial \boldsymbol{r}^e}{\partial a_k} = -\sum_e (\boldsymbol{P}^e)^T \frac{\partial \boldsymbol{r}^e}{\partial a_k} \tag{29}$$

that is, only differentiation of the element residual vector $\boldsymbol{r}^e$ is required.

In the case of a three-noded linear element, each element Ω_e can be obtained from the parent element $\hat{\Omega}$ via the mapping $\boldsymbol{\xi} \in \hat{\Omega} \mapsto \boldsymbol{x}(\boldsymbol{\xi}) \in \Omega_e$, see Figure 4. Let

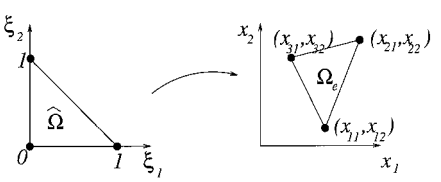

Figure 4. Parent element $\hat{\Omega}$ and the mapping $\boldsymbol{\xi}$.

$$\boldsymbol{L} = \begin{pmatrix} \dfrac{\partial \varphi_1}{\partial \xi_1} & \dfrac{\partial \varphi_2}{\partial \xi_1} & \dfrac{\partial \varphi_3}{\partial \xi_1} \\ \dfrac{\partial \varphi_1}{\partial \xi_2} & \dfrac{\partial \varphi_2}{\partial \xi_2} & \dfrac{\partial \varphi_3}{\partial \xi_2} \end{pmatrix} = \begin{pmatrix} -1 & 1 & 0 \\ -1 & 0 & 1 \end{pmatrix}$$

be the matrix of shape function derivatives for the parent element. Denoted by $\boldsymbol{J}^e$, the Jacobian of the mapping $\boldsymbol{\xi} \mapsto \boldsymbol{x}(\boldsymbol{\xi})$. Finally, let

$$\boldsymbol{X}^e = \begin{pmatrix} x_{11} & x_{12} \\ x_{12} & x_{22} \\ x_{13} & x_{23} \end{pmatrix}$$

be the matrix containing the nodal co-ordinates of Ω_e. At a point $\boldsymbol{x}(\boldsymbol{\xi}) \in \Omega_e$, the matrix $\boldsymbol{G} = \{g_{ij}\}$ of Cartesian derivatives of the shape functions is given by $\boldsymbol{G}^e(x) = (\boldsymbol{J}^e)^{-1}\boldsymbol{L}$ and the Jacobian by $\boldsymbol{J}^e = \boldsymbol{L}\boldsymbol{X}^e$.

The partial derivatives of shape function derivatives $\boldsymbol{G}$ and the determinant $\det \boldsymbol{J}$ with respect to design variables are given by

$$\frac{\partial \boldsymbol{G}}{\partial a_k} = -\boldsymbol{G}\left(\frac{\partial \boldsymbol{X}^e}{\partial a_k}\right)\boldsymbol{G} \tag{30}$$

$$\frac{\partial}{\partial a_k}(\det \boldsymbol{J}) = \det \boldsymbol{J} \sum_{i=1}^{2} \sum_{j=1}^{3} g_{ij}\left(\frac{\partial \boldsymbol{X}^e}{\partial a_k}\right)_{ji} \tag{31}$$

Now, calculation of $\partial \boldsymbol{r}^e / \partial a_k$ in Equation (29) requires differentiation of the terms like

$$\int_{\Omega_e} \frac{\partial \varphi_i}{\partial x_l} \frac{\partial \varphi_j}{\partial x_m} \, \mathrm{d}x = \frac{1}{2} g_{li} g_{mj} \det \boldsymbol{J}^e \tag{32}$$

with respect to design variables a_k.

We assume further that the topology of the finite element mesh is fixed (i.e., the number of elements and nodes together with the element connectivity are independent of a). Then, the mapping $\boldsymbol{a} \to \boldsymbol{X}(\boldsymbol{a})$ is smooth and the terms $\partial \boldsymbol{X}^e / \partial a_k$ are well defined.

4.3. Algorithm

The previous considerations lead us to the following algorithm to calculate the gradient of the cost function by the adjoint equation technique:

Algorithm 1
Given a design $\boldsymbol{a}$, compute $F(\boldsymbol{a})$ and $\nabla_{\boldsymbol{a}} F(\boldsymbol{a})$:

1. Generate a new finite element mesh $\boldsymbol{X} = \boldsymbol{X}(\boldsymbol{a})$.
2. Solve the flow problem $\boldsymbol{r}(\boldsymbol{q}) = 0$ by using the Newton–Raphson method.
3. Compute the cost $F(\boldsymbol{q})$ and the gradient $\nabla_{\boldsymbol{q}} F(\boldsymbol{q})$.

4. Solve the adjoint equation $\boldsymbol{H}(\boldsymbol{q})^T\boldsymbol{p} = \nabla_{\boldsymbol{q}} F(\boldsymbol{q})$.
5. **do** $k = 1$, N (number of design variables)
   (a) Set $\dfrac{\partial F}{\partial a_k} := 0$.
   (b) Compute $\dfrac{\partial \boldsymbol{X}}{\partial a_k}$, the partial derivatives of nodal co-ordinates with respect to design variables.
   (c) **do** $e = 1$, *nelems* (number of elements)
      (i) Compute $\dfrac{\partial \boldsymbol{G}^e}{\partial a_k}$, $\dfrac{\partial(\det \boldsymbol{J}^e)}{\partial a_k}$ using Equations (30) and (31).
      (ii) Compute $\dfrac{\partial \boldsymbol{r}^e}{\partial a_k}$.
      (iii) Set $\dfrac{\partial F}{\partial a_k} := \dfrac{\partial F}{\partial a_k} - \boldsymbol{p}^{eT}\dfrac{\partial \boldsymbol{r}^e}{\partial a_k}$.
   (d) **end do**
6. **end do**

5. NUMERICAL EXAMPLES

The resulting algorithm is used for optimization of the header geometry. Note that the examples below do not correspond to any existing headbox design.

5.1. The model problem

We first describe the dimensions for the header as in Figure 3. The fixed size parameters are: $H_1 = 1.0$, $H_2 = 0.12$, $L_1 = 1.5$, $L_2 = 8.0$ and $L_3 = 0.7$ m. The cost function is given by Equation (16) and it is minimized by varying the shape of the back wall $S(\alpha)$.

The physical parameters are chosen as follows: the density $\rho = 1000$ kg m^{-3}, the viscosity $\mu_0 = 0.001$ Pa s, the coefficients of the outflow boundary conditions, see Equation (14), $c = 1000.0$ and the inflow velocity is fixed to $\boldsymbol{u}_{\text{in}} = (u_{\text{in}}, 0.0)$ with $u_{\text{in}} = 4.0$ m s^{-1}. The recirculation flow $\boldsymbol{u}_{\text{r}} = (u_{\text{r}}, 0.0)$ will be given below.

5.2. Computer realization

The state problem (1)–(14) discretized by the stabilized finite element method on a mesh of 3960 triangular elements (2128 mesh nodes). The mesh is compatible with the boundary layer determination (5), where d is chosen equal to 5. The number of design parameters was chosen equal to 16. The resulting non-linear algebraic system (19) is linearized using the Newton–Raphson method (20); the parameter in the termination criterion for the method is chosen equal to $\epsilon_1 = 10^{-6}$. The linear systems arising from the linearization of the stabilized problem (17) were solved by a direct method based on the LU-factorization of the coefficient matrix. The resulting optimization problem (15) was solved by the SQP algorithm E04UCF from the

NAG sub-routine library [26], with the parameter in the termination criterion $\epsilon_2 = 10^{-4}$. All computations were done in double precision on a HP9000/J280 computer.

5.3. Results of experiments

In the first example, we assume the recirculation flow to be 7 per cent of the total inflow, i.e., $u_r = 2.33\ \mathrm{m\,s^{-1}}$. The desired outflow is a constant flow rate across the whole length of the outlet boundary. As an initial guess, we assume a linear back wall, i.e., the optimization is started from a linearly tapering header. It took 12 optimization iterations and 175 s of CPU time to reach the prescribed accuracy. The required number of Navier–Stokes (linearization) iterations within the optimization was between 5 and 11. The initial and the optimized back walls and the corresponding pressure profiles are given in Figure 5. In Figure 6, the initial, the optimized and the desired outlet velocity profiles are reported in a dimensionless form.

We notice from the figures that by changing the geometry via the optimization process, we can remarkably improve the outlet velocity profile, which is, in this case, rather close to the desired one.

In the second example, we assume a non-constant goal for the outflow at the boundary Γ_{out}. Again, a linear back wall is used as an initial guess for optimization. In this case, it now took seven optimization iterations and 230 s of CPU time to reach the prescribed accuracy. The required number of Navier–Stokes (linearization) iterations within the optimization was between 6 and 11. The initial and the optimized back walls and the corresponding pressure

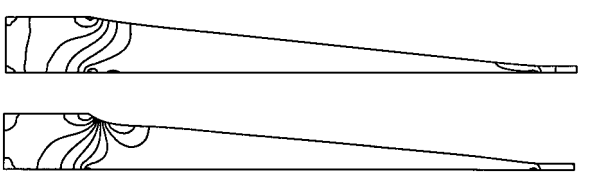

Figure 5. Example 1: pressure fields with initial and optimized geometries.

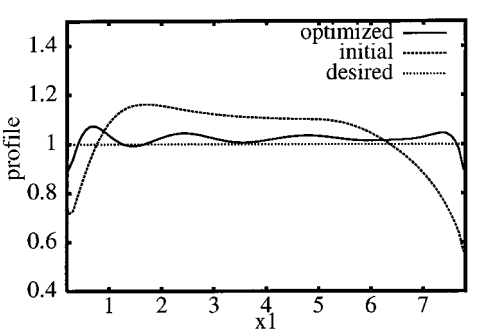

Figure 6. Example 1: outlet velovity profiles.

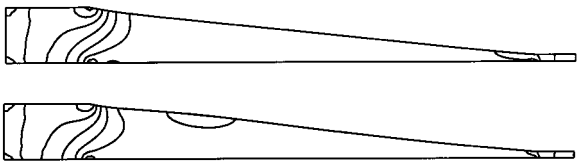

Figure 7. Example 2: pressure fields with initial and optimized geometries.

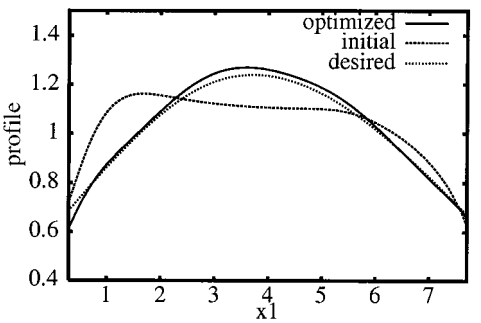

Figure 8. Example 2: outlet velocity profiles.

profiles are given in Figure 7. The original, the optimized and the desired outlet velocities are given in Figure 8. Again, same observations can be made concerning the improvement of outlet velocitites.

6. CONCLUSIONS

The numerical tests show that improved designs according to a chosen cost functional can be obtained. One SQP iteration usually required only one evaluation of the cost functional and, therefore, the total number of necessary flow problem solutions can be kept moderate. The sensitivity formulae can be rather easily programed provided that explicit expressions for the dependence of nodal co-ordinates on the design variables are available. These formulae can be extended, with obvious modifications, for higher-order elements, too.

In order to find the best possible design of the headbox in practice, attention has to been paid to the formulations of both an accurate fluid flow model and a cost function. Modeling of turbulence and, especially, for a mixture of water and wood fibers is still an unsolved problem in fluid dynamics. Furthermore, it is not always easy to determine a desired design, taking into account fluid dynamics and manufacturing aspects. However, the numerical experiments showed that shape optimization can be used to reach improved properties in an industrial flow model.

ACKNOWLEDGMENTS

This research was partially supported by the Academy of Finland (Grant 34063). The authors would also like to thank the Technology Development Center of Finland (TEKES) for their financial support of this work.

REFERENCES

1. Hämäläinen J. Mathematical modelling and simulation of fluid flows in the headbox of paper machines. Report 57 (Doctoral thesis), University of Jyväskylä, 1993.
2. Hämäläinen J, Tiihonen T. Flow simulation with homogenized outflow boundary conditions. In *Finite Elements in Fluids*, Morgan K, Oñate E, Periaux J, Peraire J, Zienkiewicz O (eds). Centro Internacional de Métodos Numéricos en Ingeniería: Barcelona, 1993; 537–545.
3. Hämäläinen J, Tiihonen T. Modelling and simulation of fluid flows in a paper machine headbox. In *ICIAM-95—Third International Congress on Industrial and Applied Mathematics*, *Issue 4: Applied Sciences*, *Especially Mechanics (Minisymposia)*, Kreuzer E, Mahrenholtz O (eds). Akademie Verlag: Berlin, 1996; 62–66.
4. Haslinger J, Neittaanmäki P. *Finite Element Approximation for Optimal Shape*, *Material and Topology Design*. Wiley: Chichester, 1996.
5. Pironneau O. *Optimal Shape Design for Elliptic Systems*. Springer: New York, 1984.
6. Angrand F. Optimum design for potential flows. *International Journal for Numerical Methods in Fluids* 1983; **3**: 265–282.
7. Beux F, Dervieux A. Exact-gradient shape optimization of a 2D Euler flow. *Finite Elements and Analytical Design* 1992; **12**: 281–302.
8. Burgreen G, Baysal O. Three-dimensional aerodynamic shape optimization of wings using sensitivity analysis. AIAA Paper No. 94-0094, 1994.
9. Hou G, Taylor A, Korivi V. Discrete shape sensitivity equations for aerodynamic problems. *International Journal for Numerical Methods in Engineering* 1994; **37**: 2251–2266.
10. Lambert P, Lecordix J, Braibant V. Constrained optimization of nacelle shapes in Euler flow using semianalytical sensitivity analysis. *Structural Optimization* 1995; **10**: 239–246.
11. Glowinski R, Pan T, Kearsley A, Periaux J. Numerical simulation and optimal shape for viscous flows by a fictitious domain method. *International Journal for Numerical Methods in Fluids* 1995; **20**: 695–711.
12. He B, Ghattas O, Antaki J, Dennis T. Shape optimization of Navier–Stokes flows with application to optimal design of artificial heart components. AIAA Paper No. 94-4387, 1994.
13. Kim D, Kim M. Minimum drag design in two-dimensional viscous flows. *International Journal for Numerical Methods in Fluids* 1995; **21**: 93–111.
14. Svenningsen K, Madsen J, Hassing H, Pauker W. Optimization of flow geometries applying quasianalytical sensitivity analysis. *Applied Mathematical Modelling* 1996; **20**: 214–224.
15. Carle A, Green L, Bischof C, Newman P. Applications of automatic differentiation in CFD. CRPC-TR94404, Center for Research on Parallel Computation, Rice University, 1994.
16. Mohammadi B. Mesh adaptation and automatic differentiation for optimal shape design. *International Journal for Computational Fluid Dynamics* 1998; **10**: 199–211.
17. Franca L, Frey S. Stabilized finite element methods: II. The incompressible Navier–Stokes equations. *Computing Methods in Applied Mechanics and Engineering* 1992; **99**: 209–233.
18. Andersson H, Benocci C. An improved pressure iteration technique for the SOLA algorithm. In *Numerical Methods in Laminar and Turbulent Flow*, *Part 1*, Taylor C, Olson M, Gresho P, Habashi W (eds). Pineridge Press: Swansea, 1985; 364–375.
19. Rodi W. *Turbulence Models and Their Application in Hydraulics*. International Association for Hydraulic Research: Delft, 1984.
20. Hämäläinen J, Tarvainen P. Numerical comparison of turbulence models for 2D-header flows. In *Final Report of the Project 'Optimization in Computational Fluid Dynamics'*, *Part IV*. Valmet Corporation–University of Jyväskylä, 1998.
21. Tarvainen P, Mäkinen R, Hämäläinen J. Shape optimization for laminar and turbulent flows with applications to geometry design of paper machine headboxes. In *Proceedings of Tenth International Conference on Finite Elements in Fluids*, Hafez M, Heinrich J (eds). University of Arizona: Tucson, AZ, 1998; 536–541.
22. Bartels R, Beatty J, Barsky B. *An Introduction to Splines for Use in Computer Graphics and Geometric Modeling*. Kaufmann: Los Altos, 1987.

23. Schittkowski K. Mathematical optimization: an introduction. In *Software Systems for Structural Optimization*, Hörnlein R, Schittkowski K (eds). Birkhäuser: Basel, 1993; 33–42.
24. Mäkinen R. Finite element design sensitivity analysis for non-linear potential problems. *Communications in Applied Numerical Methods* 1990; **6**: 343–350.
25. Mäkinen R. Optimal shape design for transonic potential flows. In *Finite Elements in Fluids*, Morgan K, Oñate E, Periaux J, Peraire J, Zienkiewicz O (eds). Centro Internacional de Métodos Numéricos en Ingeniería: Barcelona, 1993; 457–466.
26. Numerical Algorithms Group. *NAG Fortran Library*, *Mark 18*. The Numerical Algorithms Group Limited: Oxford, 1997.

